Following spinal cord injury, PDE4B drives an acute, local inflammatory response and a chronic, systemic response exacerbated by gut dysbiosis and endotoxemia

Scott A. Myers[a,b,1], Leila Gobejishvili[d,1], Sujata Saraswat Ohri[a,b], C. Garrett Wilson[e], Kariena R. Andres[a,b], Amberly S. Riegler[a,b], Hridgandh Donde[d], Swati Joshi-Barve[d], Shirish Barve[d,*], Scott R. Whittemore[a,b,c,**]

[a] Kentucky Spinal Cord Injury Research Center, University of Louisville, School of Medicine, 511 S. Floyd St., MDR 616, Louisville, KY 40202, USA
[b] Department of Neurological Surgery, University of Louisville, School of Medicine, 511 S. Floyd St., MDR 616, Louisville, KY 40202, USA
[c] Department of Anatomical Science & Neurobiology, University of Louisville, School of Medicine, 511 S. Floyd St., MDR 616, Louisville, KY 40202, USA
[d] Departments of Internal Medicine and Pharmacology and Toxicology, and Alcohol Research Center, University of Louisville, School of Medicine, 505 South Hancock Street, CTR Building, Room 515, Louisville, KY 40202, USA
[e] UAB School of Medicine, University of Alabama at Birmingham, Bevill Biomedical Research Building, Birmingham, AL 35294, USA

ARTICLE INFO

ABSTRACT

Emerging evidence links changes in the gut microbiome and intestinal barrier function to alterations in CNS function. We examined the role of endotoxin-responsive, cAMP-specific, *Pde4* subfamily *b* (*Pde4b*) enzyme in gut dysbiosis induced neuro-inflammation and white matter loss following spinal cord injury (SCI). Using a thoracic contusion model in C57Bl/6 wild type female mice, SCI led to significant shifts in the gut bacterial community including an increase in the phylum *Proteobacteria*, which consists of endotoxin-harboring, gram-negative bacteria. This was accompanied by increased systemic inflammatory marker, soluble CD14, along with markers of the endoplasmic reticulum stress response (ERSR) and inflammation in the SCI epicenter. Deletion of *Pde4b* reduced epicenter expression of markers for the ERSR and inflammation, at both acute and chronic time points post-SCI. Correspondingly, expression of oligodendrocyte mRNAs increased. Within the injury penumbra, in-flammatory protein markers of activated astrocytes (GFAP), macrophage/microglia (CD11b, Iba1), and the proinflammatory mediator Cox2, were decreased in *Pde4b*$^{-/-}$ mice. The absence of *Pde4b* improved white matter sparing and recovery of hindlimb locomotion following injury. Importantly, SCI-induced gut dysbiosis, bacterial overgrowth and endotoxemia were also prevented in *Pde4b*$^{-/-}$ mice. Taken together, these findings indicate that PDE4B plays an important role in the development of acute and chronic inflammatory response and consequent recovery following SCI.

1. Introduction

Over 10,000 individuals in the U.S. suffer traumatic SCI annually, and an estimated six million people currently live with paralysis (christopherreeve.org). In addition to the loss of limb function, acute and chronic pathophysiological changes alter organ function, including bowel function (Lynch et al., 2001) and gut dysbiosis (Kigerl et al., 2016). These changes, combined with an increase in sedentary lifestyle,

lead to obesity (Gater Jr., 2007). These metabolic pathologies can lead to metabolic syndrome, which affects > 55% of patients (Nelson et al., 2007). Bowel dysfunction, in particular, exacerbates these metabolic changes and leads to both peripheral and central chronic inflammation (Sun & Chang, 2014; Schippa & Conte, 2014; Peterson et al., 2015).

The intestinal microbiota comprise > 99% of the bacterial mass in the body and are the principal source of pathogen-associated molecular patterns in many diseases. Only trace quantities of gut bacteria and

bacterial products, such as lipopolysaccharide (LPS), reach the portal circulation under normal conditions. Gut dysbiosis develops, following a blunt insult, when the composition of the gut microbiota is changed such that pro-inflammatory, pathogenic bacteria overwhelm non-pathogenic and/or beneficial gut bacteria. Dysbiosis causes increased intestinal endotoxin production and bacterial translocation, in which gut bacteria and bacterial products migrate from the intestinal lumen into extra-intestinal sites (Joscelyn & Kasper, 2014), likely leading to chronic systemic inflammatory responses. Gut microbiome changes have been linked to alterations in CNS function (Liu et al., 2004; Burokas et al., 2015; Bienenstock et al., 2015; Mayer et al., 2015; Li & Zhou, 2016; Klingelhoefer & Reichmann, 2015; Mulak & Bonaz, 2015; Nemani et al., 2015) and SCI triggers dysbiosis (Kigerl et al., 2016).

Cyclic AMP (cAMP) is a regulator of microglia homeostasis and inflammatory cytokine expression (Ghosh et al., 2012; Laskin & Pendino, 1995). cAMP levels are critically regulated by phosphodiesterases (PDEs) which degrade cAMP and modulate cAMP signaling (Pearse & Hughes, 2016; Lugnier, 2006). Of the cAMP-specific PDEs, the PDE4 family is the preferred therapeutic target for the treatment of inflammatory diseases, depression, and cognitive deficits (Spina, 2008; Houslay, 2010). *Pde4* represents a large family, with 4 genes (*Pde4a/b/c/d*) encoding over 20 distinct isoforms. PDE4B is essential in LPS-induced tumor necrosis factor α (TNFα) production (Jin & Conti, 2002; Jin et al., 2005). Microglia detect endotoxin through toll-like receptor 4 (TLR4), leading to production of inflammatory cytokines TNFα, interleukin 1 (IL1), and nitric oxide (Laskin & Pendino, 1995; Buttini et al., 1997; Zhang et al., 2002), which contribute to neuronal damage. Peripheral inflammation leads to increased monocyte chemoattractant protein (MCP1) levels, which mediates immune cell infiltration into the CNS (D'Mello et al., 2009). The nonspecific PDE4 inhibitor rolipram attenuates microglial activation in response to endotoxin (Ghosh et al., 2012; Buttini et al., 1997; Kiebala & Maggirwar, 2011; Schaal et al., 2012; Sebastiani et al., 2006). There are conflicting reports as to whether rolipram can enhance functional recovery after contusive SCI (Schaal et al., 2012; Koopmans et al., 2009; Whitaker et al., 2008; Iannotti et al., 2011; Costa et al., 2013; Beaumont et al., 2009). While these studies implicate a role of PDE4 in glial activation, white matter loss, axonal degeneration, and inflammation, the ability of rolipram to non-selectively inhibit all members of the PDE4 family precludes the ability of these studies to identify the isoform(s) most responsible for these secondary processes post-SCI.

We hypothesized that intestinal microbiome dysbiosis, which is known to increase gut permeability and peripheral endotoxemia, activates the TLR4/TNFα/PDE4B axis and drives acute changes in neural function after SCI. This upregulation of PDE4B, in turn, leads to chronic dysfunction in metabolic status after SCI, feeding forward to exacerbate inflammation and limit functional recovery. We used *Pde4b*$^{-/-}$ mice (Blake et al., 2017) in a contusive thoracic model of SCI to investigate the role of PDE4B in neuroinflammation and white matter loss post-injury.

2. Materials and methods

2.1. Surgical procedures

All surgical intervention, care, and treatment of animals were in strict accordance with the PHS Policy on Humane Care and Use of Laboratory Animals (National Research Council, 2015) and University of Louisville Institutional Animal Care and Use Committee and Institutional Biosafety Committee guidelines, with the exception that all animals received no antibiotic treatment post-operatively. The genetic background of all strains used in this study was C57BL/6. At most, 4 mice were housed per cage, and all individuals were housed with members of the same experimental group to avoid coprophagic cross-contamination. *Pde4b*$^{-/-}$ mice (generated by Dr. Marco Conti, UCSF, San Francisco, CA) and WT littermates were housed and bred under

similar conditions in University of Louisville animal facility. Adult female mice (6–8 weeks old, 18–22 g) were anesthetized using a 2.0% avertin solution (2,2,2-tribromoethanol) administered at 240 mg/kg intraperitoneally (IP) and prepared as described (Benton et al., 2008). All mice received either sham T9 laminectomies or 50 kdyn contusions using the IH impactor (Infinite Horizons Inc., Lexington, KY) as described (Benton et al., 2008; Mahoney et al., 2009; Scheff et al., 2003). Moderate contusions were chosen to maximize the likelihood of detection of either improvement or further deficit of functional recovery following therapeutic intervention, as they produce injuries that consistently yield functional deficits that plateau within the middle of the Basso Mouse Scale (BMS). For functional assessment, mice were scored by the BMS (Basso et al., 2006) one week prior to surgery and weekly after SCI. All raters were trained and certified at Ohio State University by Dr. Basso and were blinded to genotype and/or treatment group.

2.2. TreadScan® analysis

Recording and analysis of mice placed on a motor-driven translucent treadmill were performed as described (Beare et al., 2009), except the blinded scorer set the treadmill at the best walking speed for each untrained mouse, as determined by slowly increasing the treadmill speed until the animal was consistently walking with minimal lateral/longitudinal movement (Beare et al., 2011). Locomotion was recorded from below at 100 frames/s, and TreadScan® software (CleverSys, Reston, VA) was used to track and quantify overall run speed, mean instantaneous, hindlimb swing time, stride length, toe spread, and front and rear track width. Baseline TreadScan® analysis was performed 3 days prior to injury. Terminal TreadScan® analysis was performed at 6 weeks post-SCI.

2.3. Quantitative polymerase chain reaction (qPCR)

Total RNA was extracted from spinal cord tissue of sham and contused mice ($n = 4$/group) from the injury epicenter (4 mm) at 3 h, 2 days, and 42 days post-contusion using Trizol (Invitrogen, Carlsbad, CA) according to the manufacturer's instructions. Total RNA was quantified by UV spectroscopy and RNA integrity was confirmed on an ethidium bromide stained formaldehyde agarose gel. cDNA was synthesized with 1 µg of total RNA using the High Capacity cDNA Synthesis Kit (Applied Biosystems, Foster City, CA) in a 20 µl reaction volume. As controls, mixtures containing all components except the reverse transcriptase enzyme were prepared and treated similarly. All cDNAs and control reactions were diluted 10× with nuclease-free water before using as a template for qPCR.

qPCR was performed using an ABI 7900HT Real-time PCR instrument (Applied Biosystems, Foster City, CA). Briefly, diluted cDNAs were added to Taqman universal PCR master mix and run in triplicate. Target and reference gene PCR amplification was performed in separate tubes with Assay on Demand™ primers (Applied Biosystems, Foster City, CA) as follows: *Atf4* (Mm00515324_m1), *Chop* (Mm01135937_g1), *Claudin 11* (Mm00500915_m1), *Gadd34* (Mm00492555_m1), *Grp78* (Mm01333323_g1), *Mbp* (Mm00521980_1), *Olig2* (Mm01210556_m1), *Xbp1* (Mm00457359_m1), *Nse* (Mm00468052_m1), *Map2* (Mm00485230_m1), *Gfap* (Mm00546086_m1), *CD45* (Mm01293577_m1), *Ccl2* (Mm00441242_m1), *Tnfα* (Mm00443258_m1), *Il-1β* (Mm00434228_m1), *Il6* (Ms00446190_m1), and *Atf6α* (Mm01295325_m1). The RNA levels were quantified using the ΔΔCT method. Expression values obtained from triplicate runs of each cDNA sample were normalized to triplicate value for *Gapdh* (reference gene, 4352661) from the same cDNA preparation. Transcript levels are expressed as fold changes compared with respective levels in sham or uninjured controls as indicated. For qPCR analysis of the PDE4 subfamily, protocols and primers were used as previously described (Gobejishvili et al., 2011).

Table 1
List of antibodies used for immunohistochemical staining.

Antigen/clone	Antibody type	Catalog #	Dilution	Vendor
PDE4B	prb	ab14611	1:200	Abcam, Cambridge, MA
NeuN	pgp	ABN900	1:200	Millipore, Billerica, MA
Olig2	pg	sc-19969	1:200	Santa Cruz, CA
GFAP	pc	AB5541	1:500	Millipore, Billerica, MA
Cox2	pm	160126	1:200	Cayman Chem, MI
CD11b/c	mr	553311	1:200	BD Biosciences, CA
Iba1	prb	019-19741	1:200	Wako, Richmond, VA
Mouse IgG isotype control	–	08-6599	–	Invitrogen, Carlsbad, CA
Rabbit IgG isotype control	–	08-6199	–	Invitrogen, Carlsbad, CA
Rat IgG isotype control	–	ab37361	–	Abcam, Cambridge, MA
Chicken IgY isotype cntrl	–	sc-2718	–	Santa Cruz, CA

prb = polyclonal rabbit; mr = monoclonal rat; mm = monoclonal mouse; pg = polyclonal goat; pc = polyclonal chicken; pgp = polyclonal guinea pig.

2.4. Tissue processing and immunohistochemistry

At the end of the experiment, mice were anesthetized IP with a 2.0% avertin solution (240 mg/kg). Spinal cords were dissected, frozen on dry ice, and longitudinally sectioned at 20 μm on a cryostat. Sections were thaw mounted on microscope slides (Fisher Scientific, Pittsburgh, PA) and stored at −80 °C. Slides were warmed at 37 °C for 10 min and fixed in ice-cold methanol for 20 min. Spinal cord sections were blocked in TBS + 0.1% Triton X-100, 0.5% BSA, and 10% normal donkey serum for 1 h at 25 °C and then incubated overnight at 4 °C with primary antibodies (Table 1) in a blocking buffer, followed by incubation in secondary antibodies at 25 °C for 1 h. Negative controls included appropriate species-specific non-immune Ig subtypes instead of primary antibodies. TRITC (1:200)-, FITC (1:200)-, CY5 (1:200) or AMCA (1:100)-conjugated donkey secondary antibody F(ab′)2 fragments and normal donkey serum (017-000-121) were purchased from Jackson Immunoresearch (West Grove, PA).

For the assessment of white matter sparing, animals were anesthetized IP with avertin and spinal cords were dissected after transcardial perfusion with PBS and 4% PFA. Cords were submerged in 4% PFA overnight at 4 °C, stored in a 30% sucrose solution for 72 h at 4 °C, and cut serially in 20 μm coronal sections on a cryostat 1 cm caudal and rostral to the injury epicenter. Sections were thaw mounted on microscope slides and stored at −80 °C. Eriochrome cyanine staining was performed to delineate spared myelin (Scheff et al., 2003; Magnuson et al., 2005; Myers et al., 2011).

2.5. Image quantitation

All images were captured with a Nikon TE 300 inverted microscope equipped with a Spot CCD camera using identical exposure settings. For all tissue assessments, every fifth horizontal/longitudinal section (11 to 12 20 μm-thick sections) from each cord was stained and photographed with a 10× objective and stitched with Elements™ software during acquisition. Elements™ software was used to threshold baseline brightness and contrast identically for each image for all quantitative object and field measurements. The areas of the regions of interest (ROI) were centered on the contusion epicenters and quantified by a scorer blinded to genotype. The injury epicenter was defined as the domain exhibiting significant GFAP immunoreactivity (Benton et al., 2008; Whetstone et al., 2003). The injury penumbra was defined as 500 μm rostral and caudal to the epicenter (Myers et al., 2011; Fassbender et al., 2011). The mean areas quantified from the injured cords were used to define the ROIs that were used to quantify sham control cords at roughly T9 (Benton et al., 2008). To assess the presence of inflammatory markers, the total area within the injury penumbra positive for either GFAP, COX2, CD11b, or Iba1 was quantified by digital image analysis using the basic densitometric thresholding features of Elements™ software, similar to methods previously reported (Donnelly et al., 2009). Threshold values were obtained and set for each

marker and held constant for each image quantified.

2.6. Bacterial 16S rRNA gene sequencing

Methods have been adapted from those developed for the NIH-Human Microbiome Project (Aagaard et al., 2013; Gevers et al., 2012). Briefly, bacterial genomic DNA was extracted using MO BIO PowerSoil DNA Isolation Kit (MO BIO Laboratories, Carlsbad, CA). The 16S rRNA gene V4 region was amplified by PCR and sequenced in the MiSeq platform (Illumina, San Diego, CA) using the 2 × 250 bp paired-end protocol and yielding pair-end reads that overlap almost completely. The primers used for amplification contain adapters for MiSeq sequencing and single-end barcodes allowing pooling and direct sequencing of PCR products (Caporaso et al., 2012; Caporaso et al., 2010).

2.7. 16S rRNA marker gene analysis

Our 16S rRNA gene data pipeline incorporates phylogenetic and alignment-based approaches to maximize data resolution. Read pairs were de-multiplexed based on the unique molecular barcodes, and reads were merged using FASTQ-join (Erik Aronesty, 2011) in Quantitative Insights Into Microbial Ecology (QIIME). Merged reads were trimmed and a quality filter applied to the resulting merged reads. De-multiplexed and quality filtered FASTQ files were passed into the QIIME analysis pipeline. Operational taxonomic unit (OUT) tables were generated in BIOM format using a closed-reference OTU picking method. The Greengenes database was used to identify the taxonomic classification of the 16S rRNA sequence reads. Core diversity analyses were performed in QIIME, including alpha diversity (within a sample) and beta diversity (between samples). Principal coordinate analysis (PCoA) was performed using the unweighted UniFrac method in QIIME. OTU tables were sub-sampled at an even rarefaction depth of 147313 reads to control for coverage difference between samples and to ensure even sampling of the reads.

2.8. Endotoxin assay

Blood from 6 week contused mice was drawn transcardially at the time of euthanasia, and serum samples were collected after centrifugation. Plasma endotoxin levels were measured using Limulus Amebocyte Lysate test kit (Lonza, Walkersville, MD) according to the manufacturer's instructions.

2.9. Experimental design and statistical analysis

Power analyses were calculated for all outcome measures prior to the study to determine adequate sample size and power (Lenth, 2006-2009).

2.9.1. BMS

Weekly BMS scores and subscores were analyzed using repeated measures ANOVA with the main effects of week (within subjects) and group (between subjects). Following a significant main effect, Bonferroni *post hoc t*-tests for multiple comparisons were used to determine significant differences between pairs.

2.9.2. qPCR

Naïve, 3 h, and 48 h qPCR results were analyzed with two-way ANOVA (timepoint and mouse groups = between groups) followed by Bonferroni *post hoc* t-tests for multiple comparisons.

48 h and 42 day qPCR: Because numerous independent t-test comparisons of WT and KO mice for multiple markers analyzed with qPCR would increase the likelihood of a Type I error, WT and KO mice were compared within subsets of transcripts that were grouped according to function [endoplasmic reticulum stress response (ERSR), oligodendrocyte, neuronal, inflammation and other]. Repeated measure ANOVA was used to analyze 48 h and 42 day qPCR genes data separately (transcript = within groups, and mouse = between groups) followed by Bonferroni *post hoc* t-tests for multiple comparisons.

2.9.3. 16S rRNA marker gene analysis

Nonparametric, Monte Carlo permutations were used to determine *p*-values and the Bonferroni method was used for correcting multiple comparisons.

2.9.4. Spared white matter

White matter from 10 sections each rostral and caudal from the lesion epicenter, as well as epicenter, of WT and $Pde4b^{-/-}$ mice cords was quantified. To avoid a Type I error, repeated measures ANOVA was used to compare mice within rostral and caudal cord sections (cord sections/distance = within subjects; mouse group = between). The WT and $Pde4b^{-/-}$ mice were compared using Bonferroni *post hoc* t-tests for multiple comparisons following a significant main effect for Group. Epicenter group means were compared using an Independent t-test between means with unequal variance (Levene's test for equal variance).

Datasets contained missing data (*e.g.*, BMS subscores [criteria for subscore not achieved by all mice at early post-injury time points]; qPCR data) that when analyzed with standard maximum likelihood methods in repeated measures analyses results in the loss of the entire data of the mouse. A powerful and unbiased method to handle these occurrences with no loss of data was achieved using the SPSS "mixed-effects" analysis procedure which was utilized in all ANOVA procedures (Duricki et al., 2016). All data were analyzed using IBM SPSS (v.22, v24) and are represented as means and sample standard deviations (SD). The Bonferroni *post hoc* t-test output report of t critical values ($t_{(crit)}$) in SPSS are mean difference ($t_{(diff)}$) values. For all other analyses, two-tailed Student's *t*-tests assuming equal variance were performed.

3. Results

3.1. SCI-induces an acute increase in Pde4b expression

Previous studies have shown that *Pde4b* mRNA expression increases following traumatic insults such as TBI and SCI, and PDE4B protein co-localizes with inflammatory CD11b/c-positive microglia and macrophages within the area of trauma (Atkins et al., 2007; Pearse et al., 2004). We examined *Pde4* family mRNA expression in the context of mouse contusive injury. Whereas *Pde4a* ($t_{(5)} = 8.3$, $p < 0.0001$) was downregulated, only *Pde4b* was significantly upregulated 3 h following injury ($t_{(5)} = 9.1$, $p < 0.0001$; Fig. 1A). These results are also consistent with data obtained from a rat model of moderate SCI that demonstrated an early upregulation of *Pde4b* mRNA and protein expression (Ghosh et al., 2012). We further examined the expression of specific *Pde4b* isoforms affected by SCI. qPCR analysis using primers
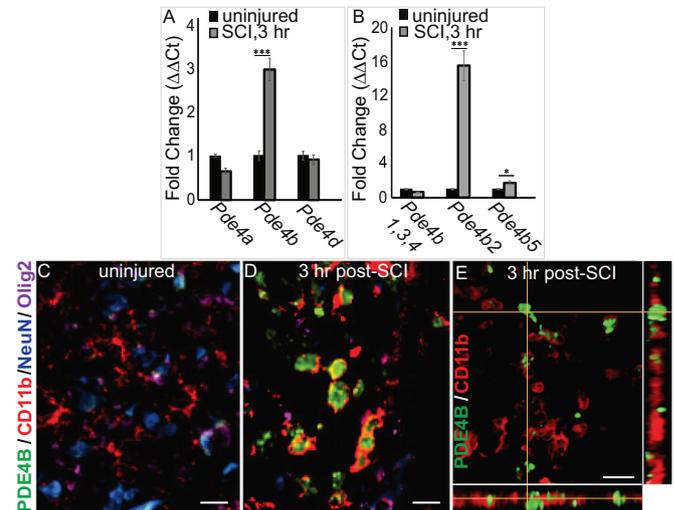

Fig. 1. *Pde4b* expression is upregulated following SCI and precedes SCI-induced systemic endotoxemia. (A) Of the 3 *Pde4* subtypes expressed in the CNS, only *Pde4b* mRNA expression is significantly upregulated 3 h following SCI ($n = 5$, *$p < 0.05$). (B) Of the long and short 5 *Pde4b* mRNA isoforms, short *Pde4b2* isoform upregulation was highest at 3 h post-SCI ($n = 5$, ***$p < 0.001$). Data are expressed as fold changes in transcript levels normalized to their respective sham controls ($\Delta\Delta$Ct). (C–E) PDE4B expression (green) primarily localizes to CD11b-positive (red) microglia/macrophage within the injury epicenter by 3 h following injury. Data are means ± S.D. ($n = 4$, *$p < 0.05$, **$p < 0.01$, ***$p < 0.001$). Bars = 100 μm. (For interpretation of the references to colour in this figure legend, the reader is referred to the web version of this article.)

selective for *Pde4b* long forms 1,3, and 4 revealed a significant downregulation in expression following SCI ($t_{(5)} = 8.2$, $p < 0.0001$; Fig. 1B). However, qPCR analysis demonstrated that SCI resulted in a robust induction of *Pde4b2* (15-fold; $t_{(5)} = 9.5$, $p < 0.0001$; Fig. 1B) and a modest induction of *Pde4b5* (1.7 fold; $t_{(5)} = 5.6$, $p = 0.002$) short forms. The expression of *Pde4b2* returned to baseline by 48 h post-SCI, and this peak expression at 3 h paralleled peak mRNA expression of key inflammatory markers, TNFα and IL-1β, within the injury epicenter (data not shown). This pattern of *Pde4b2* expression was consistent with PDE4B protein expression, which colocalized primarily with penumbral activated microglia/macrophage (Fig. 1D–G). These data are consistent with our recent study demonstrating the strong induction of *Pde4b* in primary microglia by TNFα and HMGB1 (Pilakka-Kanthikeel et al., 2012). Moreover, these peaks of expression preceded a significant increase in systemic endotoxemia at 48 h post-injury (Fig. 1C). Taken together, these results suggest that SCI-induced early induction of *Pde4b2* is not mediated by endotoxemia, but rather by inflammation and DAMPs (*e.g.* HMGB1) generated locally in the injured spinal cord.

4. SCI-induced expression of *Pde4b* plays a contributory role in the induction of acute inflammatory and ER stress responses

To examine whether PDE4B plays a contributory role in SCI-induced acute inflammation, we compared the inflammatory responses of WT to $Pde4b^{-/-}$ mice at 48 h post-injury. The epicenters of acutely injured $Pde4b^{-/-}$ mice exhibited reduced expression of the general hematopoietic marker mRNA, *CD45* ($F_{(6)} = 39.5$, $p = 0.021$, Fig. 2A), and induction of proinflammatory cytokines *Tnfα* ($F_{(6)} = 1.1$, $p = 0.009$) and *Il1β* ($F_{(16)} = 2.7$, $p = 0.022$) mRNAs were similarly lower relative to WT. The epicenters of acutely injured $Pde4b^{-/-}$ animals exhibited reduced or no induction of several ER stress mRNAs, including *Atf4* ($F_{(8)} = 0.7$, $p = 0.039$), *Grp78* ($F_{(8)} = 4.2$, $p = 0.001$), *Atf6α* ($F_{(8)} = 0.9$, $p = 0.011$), and the pro-apoptotic transcription factor, *Chop* ($F_{(8)} = 2.0$, $p = 0.014$; Fig. 2B). Whereas acutely injured epicenters exhibited no difference between WT and $Pde4b^{-/-}$ mice among the
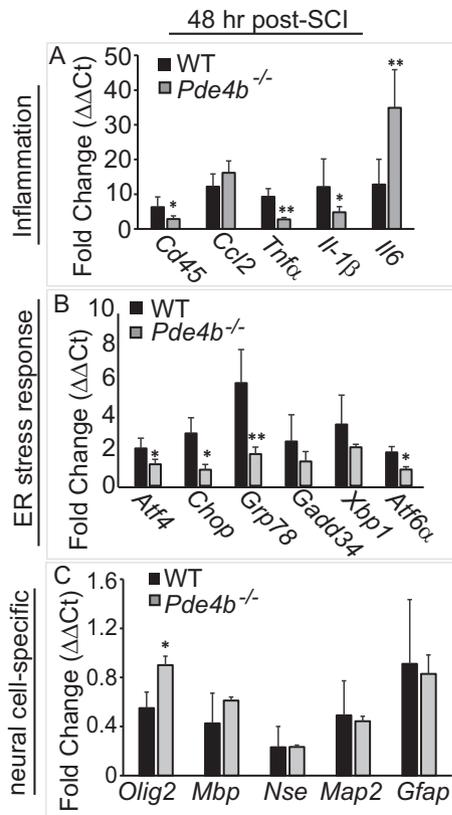
Fig. 2. Deletion of *Pde4b* reduces mRNA markers of inflammation and ER stress in the acute SCI epicenter. (A) qPCR analysis revealed significant decreases in mRNA markers for hematopoietic cells (*CD45*) and pro-inflammatory cytokines (*Tnfα* and *Il1β*) at 48 h post-SCI in *Pde4b*$^{-/-}$ mice relative to WT. (B) *Pde4b* deletion reduced ER stress mRNAs *Atf4, Chop, Grp78*, and *Atf6α* at 48 h post-injury. (C) Significantly greater preservation of *Olig2* expression was observed at 48 h post-injury in *Pde4b*$^{-/-}$ mice relative to WT. Data are means ± S.D. (n = 4, *p < 0.05, **p < 0.01, ***p < 0.001).

expression of mRNAs specific for neurons (*Nse, Map2*) or astrocytes (*Gfap*), a small but significant preservation of expression for the oligodendrocyte specific mRNA *Olig2* was observed in *Pde4b*$^{-/-}$ mice (Fig. 2C).

5. Moderate contusive SCI induces bacterial overgrowth and gut dysbiosis

Recently, in a moderate T9 spinal cord contusion model, conventional bacterial culture methods indicated the presence of bacterial overgrowth (Kigerl et al., 2016). Since bacterial overgrowth can lead to the development of intestinal barrier dysfunction (*i.e.* leaky gut), we obtained a quantitative estimation of SCI-induced bacterial overgrowth. Quantitative 16S rRNA PCR was employed that detected bacterial load across a range of 1.1×10^9 down to 0.4×10^9 16S copies/1 ng total fecal DNA. Consistently, a 2.5-fold increase in the total bacterial load as indicated by an increase in the 16S rRNA gene copy number was observed by 1 week post-SCI. This increase in bacterial growth was sustained throughout 6 weeks post-injury (Fig. 3A). In comparison. Microbial dysbiosis is also a significant feature that accompanies bacterial overgrowth and can contribute to increased intestinal endotoxin production and compromised gut barrier function, leading to increased intestinal endotoxin production, compromised gut barrier function, increased intestinal barrier permeability, and translocation of bacterial and bacterial products. These microbial and gut-associated changes can lead to peripheral endotoxemia causing activation of immune cells, chronic inflammation, and organ injury. Hence, the impact of SCI on
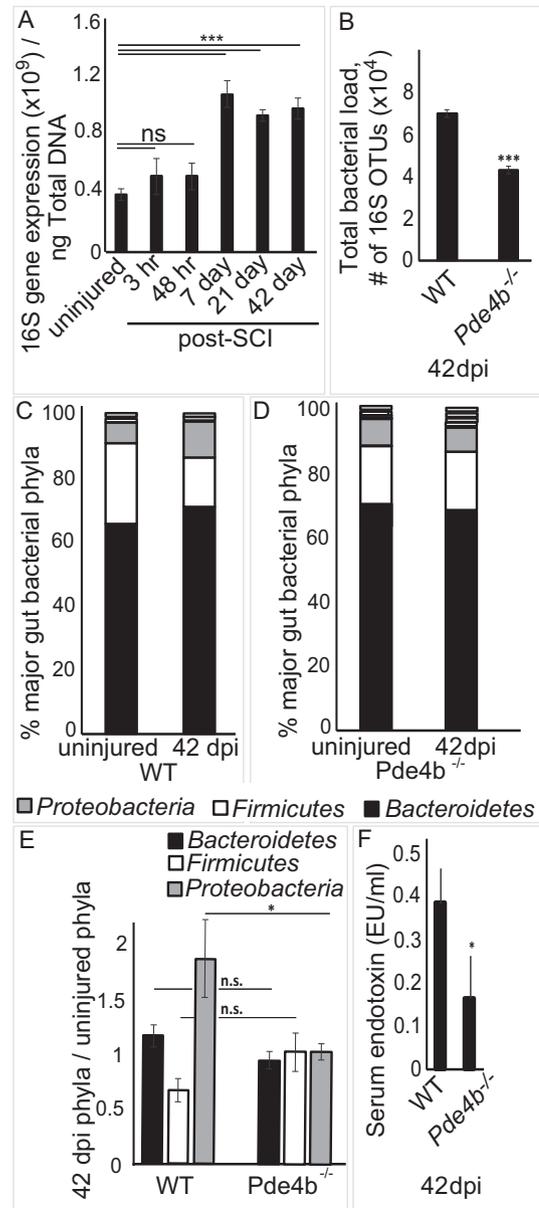

Fig. 3. SCI alters gut microbiome size and composition and increases peripheral endotoxemia in a *Pde4b*–dependent fashion. WT mice were contused, and fecal pellets were collected and analyzed at the indicated time points. Using metagenomics analysis of bacterial 16S rRNA, OTU tables were generated using a closed-reference OTU picking method. (A) Total bacterial load was significantly different from uninjured sham controls by 1 week, and up to 42 days, post-injury. Data are mean ± S.D. (n = 6, ***p < 0.001). (B) Total bacterial load (bacterial 16S operational taxonomic units (OTUs)/10 ng of fecal DNA) is lower in *Pde4b*$^{-/-}$ mice (n = 5) relative to WT (n = 5) 42 days after SCI. (C–E) The Greengenes database was used to identify the taxonomic classification of the 16S rRNA sequence reads. Core diversity analyses were performed in QIIME, including α diversity (within a sample) and β diversity (between samples). A decrease in the ratio of *Firmicutes*: *Bacteroidetes*, a measure of microbial diversity and pathology, was observed by 42 dpi in WT, but not *Pde4b*$^{-/-}$, mice. Gram-negative, endotoxin-producing *Proteobacteria* increase by 42 dpi in WT (C), but not Pde*4b*$^{-/-}$ (D), mice. Data are means (n = 6). The relative composition of *Firmicutes*, *Bacteriodetes*, and *Proteobacteria* do not change in *Pde4b*$^{-/-}$ mice 42 days post-SCI, in contrast to WT mice (E). (F) Serum endotoxin levels were decreased in *Pde4b*$^{-/-}$ (n = 5) mice relative to WT mice (n = 5) 6 weeks post-SCI. Data are means ± S.D. (*p < 0.05).

the gut microbiome composition was also examined by metagenomic analysis of the fecal DNA by amplification of the V3-V5 regions of the 16S rRNA gene and large-scale parallel pyrosequencing using the Illumina MiSeq platform and analyzed with QIIME software and Ribosomal Database Project (RDP) classifier. Significant gut microbial dysbiosis accompanied SCI-induced bacterial overgrowth. Specifically, in WT mice, SCI-induced microbial dysbiosis was characterized by an expansion of *Bacteroidetes* and a reduction of *Firmicutes* (Fig. 3C,D). *Bacteroidetes* and *Firmicutes* constitute the two major bacterial phyla of the gut microbiome and alterations in their ratio can negatively impact gut health. Moreover, the SCI-induced microbial dysbiosis was also characterized by an increase in the phylum *Proteobacteria* (Fig. 3E), which is comprised of Gram-negative bacteria that contain LPS (endotoxin) in their cell wall. It is noteworthy, that increase in *Proteobacteria* observed in many disease states correlates with increased systemic levels of endotoxin and inflammation. $Pde4b^{-/-}$ mice did not experience significant expansion in the *Proteobacteria* phylum as observed in WT mice ($t_{(13)} = 2.2$, $p = 0.0497$; Fig. 3D). Moreover, ratios of *Bacteriodetes* and *Firmicutes* remained unchanged after SCI in $Pde4b^{-/-}$ mice (Fig. 3D,E). In correlation with these lack of changes in the gut microbiome composition, plasma endotoxin levels were significantly lower in $Pde4b^{-/-}$ mice as compared to WT mice ($t_{(8)} = 2.9$, $p = 0.0171$; Fig. 3F).

6. Deletion of *Pde4b* reduces chronic inflammatory responses and lowers chronic ER stress following SCI

By 42 days post-injury, the increase in resident gut Gram-positive bacteria correlated with an increase in sCD14, a marker of systemic inflammation (Duricki et al., 2016) in WT mice ($t_{(4)} = 3.26$, $p = 0.031$, Fig. 4A). This increase was mitigated in $Pde4b^{-/-}$ mice (Fig. 4A). Whereas inflammation persisted in WT mice at 42 days after SCI, *Il-1β* ($F_{(16)} = 1.0$, $p < 0.001$) and *Tnfα* ($F_{(6)} = 1.3$, $p < 0.001$) mRNAs remained at significantly lower levels in $Pde4b^{-/-}$ mice. (Fig. 4B). The lower mRNA expression of the ER stress markers *Chop* ($F_{(9)} = 1.3$, $p < 0.0001$) and *Gadd34* ($F_{(9)} = 1.5$, $p < 0.0001$) in $Pde4b^{-/-}$ mice was also maintained in the chronically injured animals (Fig. 4B). No differences in the expression values between WT and $Pde4b^{-/-}$ uninjured animals existed among any of the markers tested, except for two involved in ER stress. Uninjured $Pde4b^{-/-}$ mice had lower expression of *Chop* (mean = 7.40, $t_{(9)} = 1.30$, $p = 0.023$) and *Grp78* (mean = 4.68, $t_{(9)} = 1.60$, $p = 0.047$) mRNAs relative to WT uninjured expression of *Chop* (8.30) and *Grp78* (5.58) mRNAs.

Forty-two days after SCI, longitudinal sections of WT and $Pde4b^{-/-}$ spinal cords were stained and quantified immunohistochemically (Table 1) to assess the effects of PDE4B on inflammation following injury. The injury penumbra of $Pde4b^{-/-}$ mice exhibited significantly less localization of GFAP$^+$ astrocytes ($p < 0.001$; post-hoc, $p = 0.005$; Fig. 5B,F,I) relative to WT (Fig. 5A,C,I), and the proinflammatory PGE$_2$-catalyzing, inducible COX2 was similarly reduced ($p < 0.001$; post-hoc, $p = 0.001$) after injury (Fig. 5B,G,J) relative to WT (Fig. 5A,G,J). $Pde4b^{-/-}$ mice expressed reduced penumbral localization of two microglial/macrophage markers, CD11b ($p < 0.001$; post-hoc, $p < 0.001$; Fig. 6B,C) and Iba-1 ($p < 0.001$; post-hoc, $p < 0.001$; Fig. 6B,D), relative to WT (Fig. 6A,C,D).

While no changes in expression of neural or astrocytic markers were observed 42 days post-injury, $Pde4b^{-/-}$ mice maintained higher levels of oligodendrocyte-specific *Olig2* ($F_{(9)} = 1.1$, $p < 0.0001$) and *Mbp* ($F_{(9)} = 0.6$, $p < 0.0001$; Fig. 4D) mRNAs. Consistent with the increased expression of *Olig2* and *Mbp* mRNAs within the injury epicenter at 42 dpi, eriochrome cyanine staining of white matter revealed a significant increase in spared white matter in the epicenters of $Pde4b^{-/-}$ mice relative to WT at 42 dpi ($t_{(5)} = 4.9$, $p = 0.001$; Fig. 7D–F). This improvement in spared white matter persisted up to 160 μm both rostrally and caudally beyond the injury epicenter. Together, these data suggest that global *Pde4b* deletion improves sparing of oligodendrocytes within the injury epicenter.
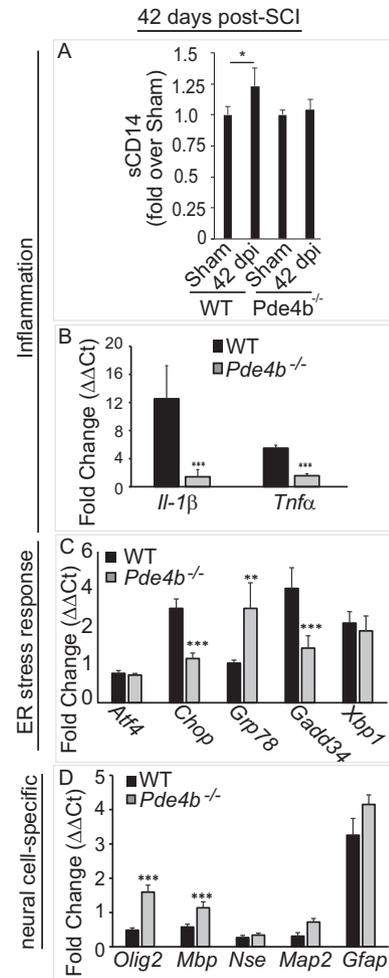

42 days post-SCI

Fig. 4. Deletion of *Pde4b* reduces markers of inflammation and ER stress in the epicenters of chronic SCI. (A) Plasma levels of sCD14 were significantly increased in WT, but not $Pde4b^{-/-}$, mice by 42 dpi. Data are mean ± S.D. (n = 6, *p < 0.05). (B) qPCR analysis revealed significant decreases in mRNA markers for the pro-inflammatory cytokines *Tnfα* and *Il1β* chronically in $Pde4b^{-/-}$ mice. (C) *Pde4b* deletion reduced the ER stress mRNAs *Chop* and *Gadd34* at 42 dpi. (D) Increased expression of *Olig2* and an mRNA marker for mature oligodendrocytes (*Mbp*) was observed at 42 dpi in $Pde4b^{-/-}$ mice. Data are expressed as fold changes in transcript levels normalized to their respective naive controls (ΔΔCt). Data are means ± S.D. (n = 4, *p < 0.05, **p < 0.01, ***p < 0.001).

7. Deletion of *Pde4b* improves functional recovery after thoracic SCI

As early as 14 dpi ($t_{(31)} = 0.56$, $p = 0.035$), $Pde4b^{-/-}$ mice showed enhanced locomotor function ($F_{(1,191)} = 57.2$, $p < 0.0001$), which was sustained through 42 days post-SCI (21 dpi, $t_{(28)} = 1.1$, $p = 0.001$; 28 dpi, $t_{(27)} = 1.4$, $p < 0.0001$; 35 dpi, $t_{(28)} = 1.0$, $p = 0.006$; 42 dpi, $t_{(28)} = 1.3$, $p = 0.004$; Fig. 7A). The increase in BMS above 5 is significant in the non-linear BMS scale, as it reflects the restoration of the capacity for plantar stepping and weight support (Basso et al., 2006). BMS subscore analysis revealed a significantly greater number of $Pde4b^{-/-}$ mice with improved motor function ($F_{(1, 5)} = 42.4$, $p < 0.0001$) beginning 14 days post-injury ($t_{(18)} = 1.9$, $p = 0.005$), with primarily an improvement in hindlimb coordination relative to WT mice throughout the experiment (21 dpi, $t_{(20)} = 2.4$, $p = 0.021$; 28 dpi, $t_{(21)} = 2.2$, $p = 0.018$; 35 dpi, $t_{(22)} = 3.0$, $p = 0.002$; 42 dpi, $t_{(22)} = 2.9$, $p = 0.012$; Fig. 7B). Impact force and displacement of the contusive injuries were not significantly different between groups and
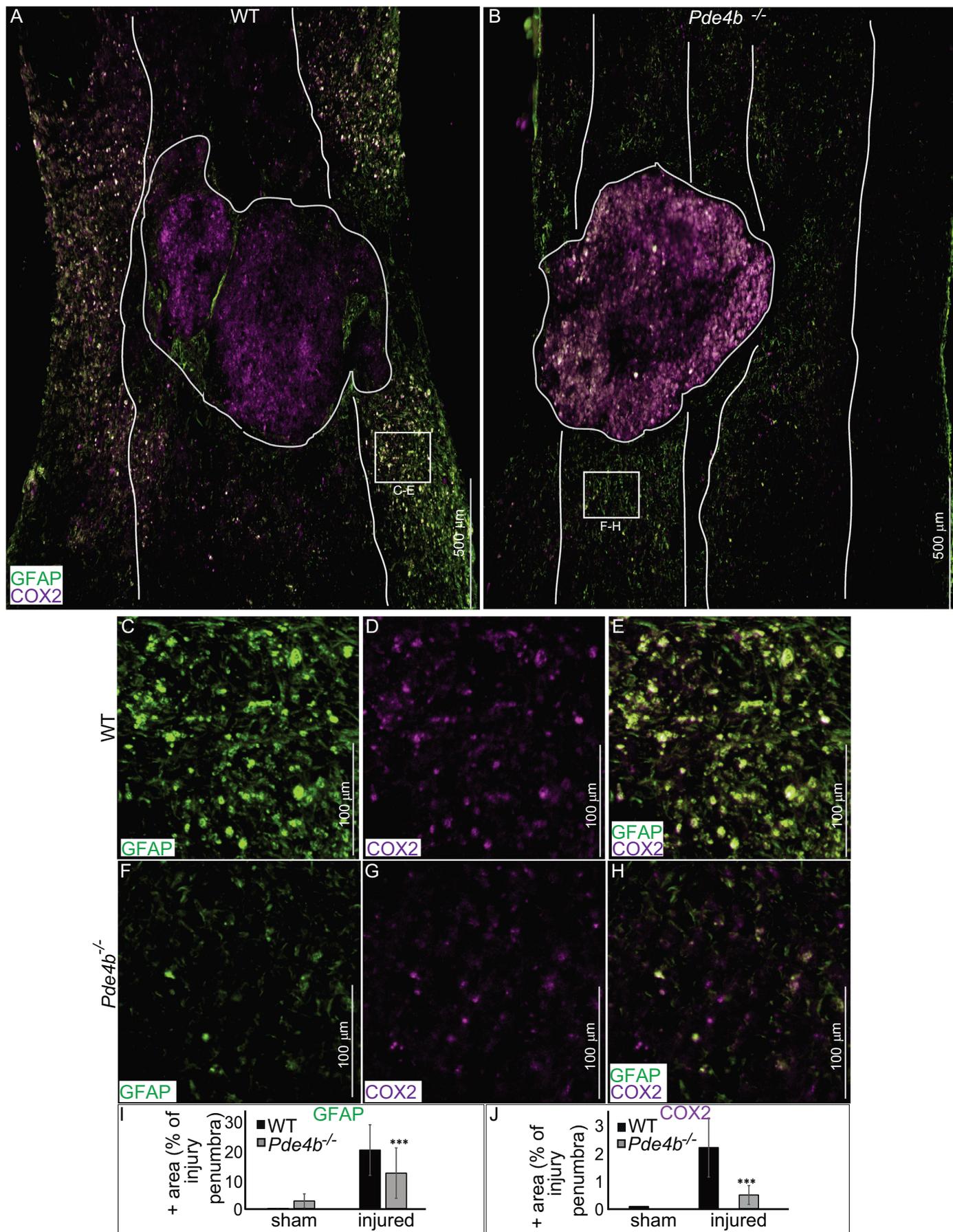
(caption on next page)

Fig. 5. *Pde4b$^{-/-}$* mice exhibit reduced penumbral inflammation 42 days following SCI. The mean percent area of the injury penumbra positive for the inflammatory markers GFAP (green; A,B,C,F,I) and COX2 (purple; A,B,D,G,J) were significantly reduced by 42 dpi in *Pde4b$^{-/-}$* mice (***p < 0.001). Data are ± S.D. (WT, n = 4; *Pde4b$^{-/-}$*, n = 4). Bars = 100 and 500 μm. Data are means ± S.D. (n = 4, ***p < 0.001). Epicenter borders are designated with solid lines; white/gray matter borders are designated with dashed lines. Bars = 100 μm. (For interpretation of the references to colour in this figure legend, the reader is referred to the web version of this article.)

no significant differences in morbidity or mortality rates were observed (data not shown). At 42 days post-injury, TreadScan® analysis revealed a small, but significant increase in front right stance time ($F_{(1, 14)}$ = 5.2, p = 0.039; *post-hoc*, p = 0.047) in *Pde4b$^{-/-}$* mice relative to WT mice (Fig. 7C). Additionally, an increase in front track width ($F_{(1, 25)}$ = 6.1, p = 0.021; *post-hoc*, p = 0.003) and left foot base of support ($F_{(1, 18)}$ = 5.9, p = 0.026; *post-hoc*, p = 0.001) was observed in the WT mice relative to *Pde4b$^{-/-}$* mice after injury, despite similar baseline values between groups in uninjured animals (Fig. 7C). *Pde4b$^{-/-}$* mice exhibited a reduced maximum longitudinal deviation (mean = 1.08 mm) relative to WT mice (mean = 1.19 mm) following injury ($t_{(13)}$ = 2.4, p = 0.033), as well as a decreased maximum lateral deviation (mean = 9.09 mm) relative to WT mice (mean = 11.60 mm) at 42 dpi ($F_{(1, 20)}$ = 15.6, p = 0.001; *post-hoc*, p = 0.008). Similarly, *Pde4b$^{-/-}$* mice exhibited a reduced minimum lateral deviation (mean = −0.05 mm) relative to WT (mean = 7.23) post-injury ($F_{(1, 15)}$ = 10.6, p = 0.006; *post-hoc*, p = 0.004). These increases in front track width, left foot base of support, maximum longitudinal deviation, and maximum lateral deviation after injury are consistent with a greater severity of contusion and lower BBB scores in rats (Avila et al., 2017) and, correspondingly, lower scores in *Pde4b$^{-/-}$* mice suggest a greater degree of recovery relative to WT. No significant differences were observed between groups in hindlimb swing time, stride length, rear track width, or overall run speed, either before or following injury (data not shown). Together, these data suggest that global *Pde4b* deletion improves recovery from contusive SCI and suggests that the improved sparing of oligodendrocytes and inflammation within the injury epicenter contributes to this functional recovery.

8. Discussion

Recent pre-clinical and clinical work has shown that SCI sequelae are associated with the development of gut-associated changes including gut microbial dysbiosis and barrier dysfunction (Kigerl et al., 2016; Joscelyn & Kasper, 2014; Lakatos et al., 2011). Further, pre-clinical studies in a mouse model showed that dysbiotic gut microbes negatively impact recovery of neurological function and enhances neuropathology after SCI (Kigerl et al., 2016). Although these studies implicate the role of gut dysbiosis in SCI, the underlying mechanisms that drive this pathogenesis remain largely undetermined. Gut dysbiosis

involves dynamic changes in the microbial membership that are qualitative and quantitative and disease-dependent (Krizsan-Agbas et al., 2014). Hence, to address the gut-controlled mechanisms that contribute to SCI pathogenesis, we examined the impact of SCI on gut dysbiosis. The 2.5-fold increase in 16S rDNA copy number seen at 1 week post-SCI, which was sustained throughout 42 dpi, indicates a substantial increase in total bacterial numbers. SCI patients suffer gastrointestinal (GI) function disorder (Gungor et al., 2016), which is associated with intestinal bacterial overgrowth. Further, this bacterial overgrowth could also contribute to shifts in the microbial phyla and gut microbial dysbiosis as has been recently documented in SCI patients (Lakatos et al., 2011). Besides the increase in *Bacteroidetes* and reduction in *Firmicutes*, there was a significant increase in the phylum *Proteobacteria* at 42 days post-SCI. The expansion of the phylum *Proteobacteria* is physiologically significant because it includes Gram negative bacteria, a major source of endotoxin. The *Proteobacteria* phylum includes a wide variety of pathogenic species, such as *Escherichia, Salmonella, Vibrio,* and *Helicobacter* (Carding et al., 2015).

Bacterial dysbiosis and expansion of the *Proteobacteria* phylum is linked with increased systemic endotoxemia, activation of peripheral monocytes/macrophages, and inflammation (Pan et al., 2014; Schulz et al., 2016). In the present studies, commensurate with the expansion of the *Proteobacteria* phylum and impaired gut barrier function, SCI increased plasma sCD14 (Fig. 4A). Increased release of sCD14 from monocytes occurs in response to stimulation with endotoxin and other microbial antigens (Bull-Otterson et al., 2013) and, therefore, provides evidence for direct, chronic endotoxin activation of monocytes and macrophages *in vivo*. sCD14 is also a clinical indicator of gut microbial translocation and correlates with serum bacterial 16SrDNA and systemic immune activation (Mutlu et al., 2012). Following SCI, the gut-mediated peripheral changes correlated with increased spinal cord ER stress, oligodendrocyte cytotoxicity, and locomotor functional loss. These data indicate that SCI-induced peripheral inflammation is linked to the development of CNS inflammation. Collectively, these results implicate the SCI-induced expansion of the Gram-negative *Proteobacteria* bacteria, gut barrier dysfunction, and translocation of microbial products as playing a major role in initiating and sustaining peripheral and CNS inflammation.

Previous work has shown that PDE4B plays a critical role in mediating inflammatory changes induced by endotoxin (Jin et al., 2005;
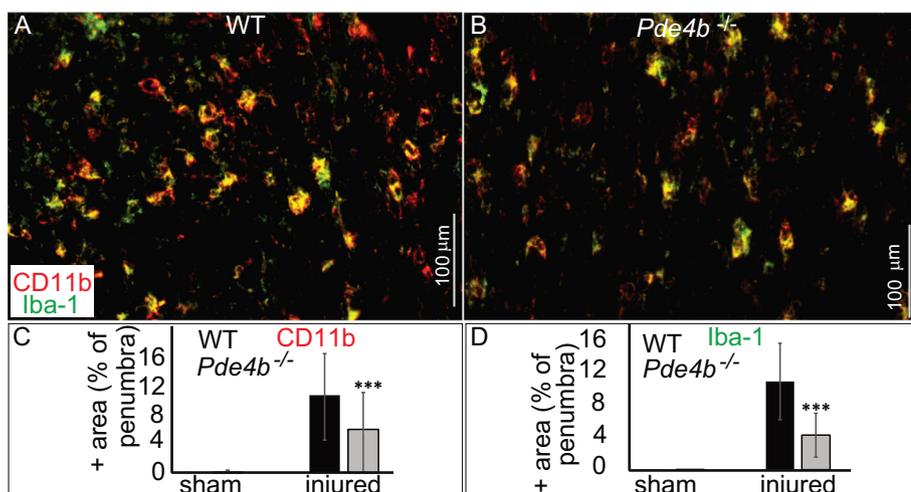

Fig. 6. *Pde4b$^{-/-}$* mice exhibit reduced penumbral activated microglia by 42 days following SCI. The mean percent area of the injury penumbra positive for the microglia markers CD11b (red; A–C) and Iba-1 (green; A,B,D) were reduced at 42 dpi in *Pde4b$^{-/-}$* mice. Data are means ± S.D. (n = 4, ***p < 0.001). Bars = 100 μm. (For interpretation of the references to colour in this figure legend, the reader is referred to the web version of this article.)
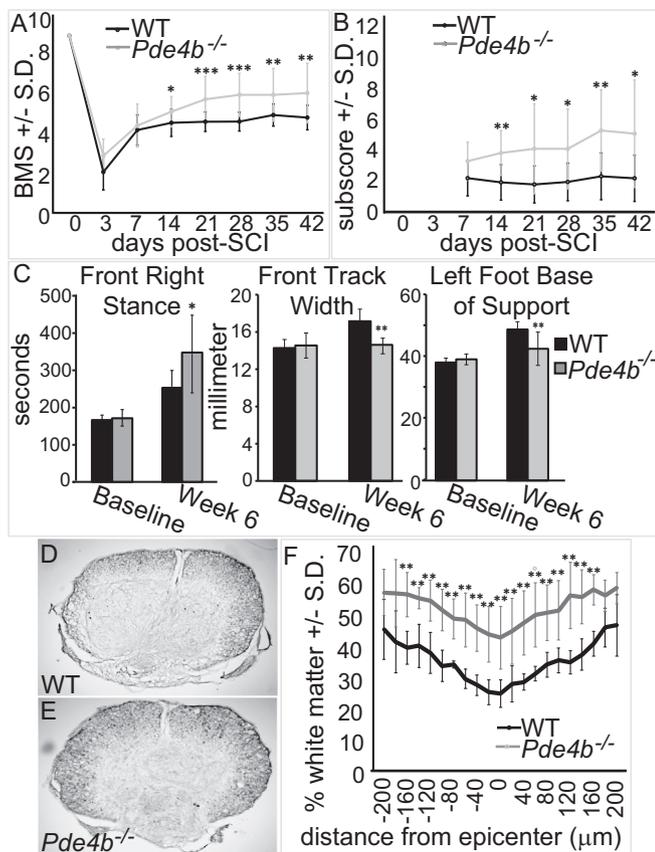
Fig. 7. Deletion of *Pde4b* improves functional recovery after moderate SCI. (A) Adult $Pde4b^{-/-}$ mice ($n = 15$) exhibited a significant improvement in hindlimb locomotor recovery by day 14 post-SCI relative to WT ($n = 19$), as assessed by the BMS (*p < 0.05, **p < 0.01, ***p < 0.001). (B) BMS subscore analysis revealed a similar improvement in hindlimb coordination (**p < 0.01, ***p < 0.001) in $Pde4b^{-/-}$ mice. (C) TreadScan® analysis indicates that $Pde4b^{-/-}$ mice exhibit increased front right stance and reduced front track width and left foot base of support 6 weeks after, but not before, injury (*p < 0.05, **p < 0.01). (D–F) Eriochrome cyanine staining demonstrated that $Pde4b^{-/-}$ mice (n = 5) exhibit significantly greater sparing of white matter within, and over 100 μm rostral and caudal, to the injury epicenter relative to WT (n = 5, *p < 0.01) at 42 dpi.

Fernandez-Real et al., 2005). More recently, we demonstrated that peripheral endotoxemia leads to brain inflammatory changes *via* induction of *Pde4b* expression (Pilakka-Kanthikeel et al., 2012). PDE4 provides the highest proportion of phosphodiesterase activity in the CNS (Gobejishvili et al., 2008). After thoracic contusive SCI, the expression of *Pde4b2* mRNA is most significantly induced. However, there are conflicting data on the effectiveness of inhibiting PDE4 with the non-selective drug rolipram as a means to improve outcomes following SCI (Pearse & Hughes, 2016; Iannotti et al., 2011; Costa et al., 2013). For example, Pearse et al. (Pearse et al., 2004) found that rolipram increased the number of central myelinated axons, while Schaal et al. (Schaal et al., 2012) found no improvement. Ianotti et al. (Iannotti et al., 2011) showed that rolipram improved white matter sparing, while Beaumont et al. (Beaumont et al., 2009) found no change. Ianotti et al. (Iannotti et al., 2011) found that rolipram improved BBB open-field hindlimb locomotor function for all 4 weeks tested, while Pearse et al. (Pearse et al., 2004) detected significant improvements in BBB scores for only a more modest 2 out of 8 weeks tested. When this experiment was repeated at a higher sub-cutaneous dose (1.2 mg/kg/day) for a longer duration (28 days), no improvement in hindlimb locomotor function was detected (Kleppisch, 2009). On the other hand, a higher sub-cutaneous regimen of 3.18 mg/kg/day for two weeks yielded the

greatest, most consistent improvement in BBB score for up to 8 weeks (Costa et al., 2013). We used $Pde4b^{-/-}$ mice to investigate secondary consequences following traumatic injury for two reasons: to avoid pharmacokinetic and pharmacodynamic issues of dosing, route of administration, as well as off-target effects (Wang et al., 2006), and to investigate the specific effects of PDE4B inhibition, rather than broad inhibition of all PDE4 isoforms. Present data indicate that it is PDE4B which plays a causal role in SCI-induced pathogenic changes including inflammation and ER stress within the spinal cord.

The decreases in inflammatory responses following SCI in $Pde4b^{-/-}$ mice may contribute to the improved oligodendrocyte sparing observed. However, it is also well established that oligodendrocytes, possessing high protein translation requirements, are particularly sensitive to injury-induced ERSR (Murphy DLA et al., 1987; Southwood et al., 2002; Lin et al., 2007; Pennuto et al., 2008; Ohri et al., 2011). Acute IL-6 mRNA levels within the spinal cord were higher in PDE4b mice relative to WT. Sustained, chronic exposure of IL-6 is pro-inflammatory *via* trans-signaling pathways; yet acute, classic-signaling of IL-6 has been shown to be involved in liver regeneration, anti-apoptotic signaling, hematopoiesis, and the protection of intestinal epithelial cells (Narazaki & Kishimoto, 2018; Scheller et al., 2011). We speculate that because IL-6 levels were not different between genotypes at 42 dpi (not shown), the chronic, pro-inflammatory effects of IL-6 were not present in $Pde4b^{-/-}$ mice, and the increased acute IL-6 levels may have contributed to the functional recovery of this genotype.

Our inflammatory response data are consistent with recent studies employing interference RNA specific to *Pde4b* (Ohri et al., 2013; Komatsu et al., 2013; Gurney et al., 2015; Ji et al., 2016) and subtype-specific, allosteric inhibitors (Gurney et al., 2015). However, consistent with studies using PDE4 antagonists, PDE4B inhibition is possibly efficacious not simply *via* its anti-inflammatory effects. PDE4B-dependent increases in neurogenesis (McGirr et al., 2016; Houslay et al., 2005), neuronal survival, neural plasticity, synaptic strengthening, and re-myelination repair (Bretzner et al., 2010) could also contribute. The increase in oligodendrocyte sparing within the epicenter of $Pde4b^{-/-}$ mice are consistent with some of these studies. Given that the behavioral deficits following a thoracic contusive injury primarily correlate with white, not gray, matter loss (Basso et al., 2006; Magnuson et al., 2005), we suggest that the increased sparing of oligodendrocytes after *Pde4b* deletion may more significantly contribute to hindlimb functional recovery. Identical conclusions were reached in studies that modified the ERSR concomitant with SCI (Pennuto et al., 2008; Ohri et al., 2011). Similarly, Bretzner et al. (Bretzner et al., 2010) reported that rolipram treatment, at a drug regimen that increased neuronal sparing, but not the number of central myelinated axons (Schaal et al., 2012), failed to improve thermal hypersensitivity or performance on the cylinder test and food-pellet reaching tasks, suggesting that oligodendrocyte sparing is more consequential than neuronal survival to functional improvement after thoracic contusive SCI.

While the use of PDE4B-selective inhibitors in preclinical studies is new, general PDE4 inhibitors have reduced neuroinflammation in many studies (Schaal et al., 2012; Atkins et al., 2007; Pearse et al., 2004; Houslay et al., 2005; Gonzalez-Garcia et al., 2013). Present data support the need to develop PDE4B-selective inhibitors, such as the PDE4B-NAMs (Komatsu et al., 2013). While the blood brain/spinal cord barrier is compromised in traumatic CNS injury, efforts to develop selective inhibitors must focus on BBB-penetrant, well-tolerated molecules that limit the nausea and emesis generated by PDE4D activation.

It is important to note that the current study is correlative and does not establish that gut dysbiosis directly exacerbates pro-inflammatory responses within the spinal cord. Dysbiotic bacterial overgrowth has been directly shown to exacerbate inflammation, lesion volume, and functional deficits following two distinct experimental stroke mouse models (Singh et al., 2016). Future studies must similarly compare recovery after SCI in germ free mice colonized with either dysbiotic or control microbiota to establish a direct, causal link between gut

dysbiosis and inflammation in the spinal cord.

9. Conclusions

What is evident from current data is that therapies targeting changes in the gut microbiome, intestinal barrier permeability, and the resultant systemic inflammatory response may limit both acute and chronic SCI-induced pathology. Probiotic treatment has abrogated inflammation in alcohol-induced liver pathology (Pan et al., 2014; Wang et al., 2011), type 2 diabetes (Wen & Duffy, 2017), inflammatory bowel disease (Holleran et al., 2017), as well as SCI-induced inflammation (Kigerl et al., 2016). Combining complementary therapies that limit initial gut dysfunction with therapies that abrogate the peripheral and central inflammatory responses may prove effective at limiting secondary cell death and chronic metabolic pathology and, ultimately, enhancing functional recovery.

Acknowledgements

Conflict of interest

The authors declare no competing financial interests.

References

Lynch, A.C., Antony, A., Dobbs, B.R., Frizelle, F.A., 2001. Bowel dysfunction following spinal cord injury. Spinal Cord 39, 193–203.

Kigerl, K.A., Hall, J.C., Wang, L., Mo, X., Yu, Z., Popovich, P.G., 2016. Gut dysbiosis impairs recovery after spinal cord injury. J. Exp. Med. 213, 2603–2620.

Gater Jr., D.R., 2007. Obesity after spinal cord injury. Phys. Med. Rehabil. Clin. N. Am. 18, 333–351 (vii).

Nelson, M.D., Widman, L.M., Abresch, R.T., Stanhope, K., Havel, P.J., Styne, D.M., McDonald, C.M., 2007. Metabolic syndrome in adolescents with spinal cord dysfunction. J. Spinal Cord Med. 30 (Suppl. 1), S127–S139.

Sun, J., Chang, E.B., 2014. Exploring gut microbes in human health and disease: pushing the envelope. Genes Dis. 1, 132–139.

Schippa, S., Conte, M.P., 2014. Dysbiotic events in gut microbiota: impact on human health. Nutrients 6, 5786–5805.

Peterson, C.T., Sharma, V., Elmen, L., Peterson, S.N., 2015. Immune homeostasis, dysbiosis and therapeutic modulation of the gut microbiota. Clin. Exp. Immunol. 179, 363–377.

Joscelyn, J., Kasper, L.H., 2014. Digesting the emerging role for the gut microbiome in central nervous system demyelination. Mult. Scler. 20, 1553–1559.

Liu, J., An, H., Jiang, D., Huang, W., Zou, H., Meng, C., Li, H., 2004. Study of bacterial translocation from gut after paraplegia caused by spinal cord injury in rats. Spine (Phila Pa 1976) 29, 164–169.

Burokas, A., Moloney, R.D., Dinan, T.G., Cryan, J.F., 2015. Microbiota regulation of the Mammalian gut-brain axis. Adv. Appl. Microbiol. 91, 1–62.

Bienenstock, J., Kunze, W., Forsythe, P., 2015. Microbiota and the gut-brain axis. Nutr. Rev. 73 (Suppl. 1), 28–31.

Mayer, E.A., Tillisch, K., Gupta, A., 2015. Gut/brain axis and the microbiota. J. Clin. Invest. 125, 926–938.

Li, Q., Zhou, J.M., 2016. The microbiota-gut-brain axis and its potential therapeutic role in autism spectrum disorder. Neuroscience 324, 131–139.

Klingelhoefer, L., Reichmann, H., 2015. Pathogenesis of Parkinson disease–the gut-brain axis and environmental factors. Nat. Rev. Neurol. 11, 625–636.

Mulak, A., Bonaz, B., 2015. Brain-gut-microbiota axis in Parkinson's disease. World J. Gastroenterol. 21, 10609–10620.

Nemani, K., Hosseini Ghomi, R., McCormick, B., Fan, X., 2015. Schizophrenia and the gut-brain axis. Prog. Neuro-Psychopharmacol. Biol. Psychiatry 56, 155–160.

Ghosh, M., Garcia-Castillo, D., Aguirre, V., Golshani, R., Atkins, C.M., Bramlett, H.M., Dietrich, W.D., et al., 2012. Proinflammatory cytokine regulation of cyclic AMP-phosphodiesterase 4 signaling in microglia in vitro and following CNS injury. Glia 60, 1839–1859.

Laskin, D.L., Pendino, K.J., 1995. Macrophages and inflammatory mediators in tissue injury. Annu. Rev. Pharmacol. Toxicol. 35, 655–677.

Pearse, D.D., Hughes, Z.A., 2016. PDE4B as a microglia target to reduce neuroinflammation. Glia 64, 1698–1709.

Lugnier, C., 2006. Cyclic nucleotide phosphodiesterase (PDE) superfamily: a new target for the development of specific therapeutic agents. Pharmacol. Ther. 109, 366–398.

Spina, D., 2008. PDE4 inhibitors: current status. Br. J. Pharmacol. 155, 308–315.

Houslay, M.D., 2010. Underpinning compartmentalised cAMP signalling through targeted cAMP breakdown. Trends Biochem. Sci. 35, 91–100.

Jin, S.L., Conti, M., 2002. Induction of the cyclic nucleotide phosphodiesterase PDE4B is essential for LPS-activated TNF-alpha responses. Proc. Natl. Acad. Sci. U. S. A. 99, 7628–7633.

Jin, S.L., Lan, L., Zoudilova, M., Conti, M., 2005. Specific role of phosphodiesterase 4B in lipopolysaccharide-induced signaling in mouse macrophages. J. Immunol. 175, 1523–1531.

Buttini, M., Mir, A., Appel, K., Wiederhold, K.H., Limonta, S., Gebicke-Haerter, P.J., Boddeke, H.W., 1997. Lipopolysaccharide induces expression of tumour necrosis factor alpha in rat brain: inhibition by methylprednisolone and by rolipram. Br. J. Pharmacol. 122, 1483–1489.

Zhang, B., Yang, L., Konishi, Y., Maeda, N., Sakanaka, M., Tanaka, J., 2002. Suppressive effects of phosphodiesterase type IV inhibitors on rat cultured microglial cells: comparison with other types of cAMP-elevating agents. Neuropharmacology 42, 262–269.

D'Mello, C., Le, T., Swain, M.G., 2009. Cerebral microglia recruit monocytes into the brain in response to tumor necrosis factoralpha signaling during peripheral organ inflammation. J. Neurosci. 29, 2089–2102.

Kiebala, M., Maggirwar, S.B., 2011. Ibudilast, a pharmacologic phosphodiesterase inhibitor, prevents human immunodeficiency virus-1 Tat-mediated activation of microglial cells. PLoS One 6, e18633.

Schaal, S.M., Garg, M.S., Ghosh, M., Lovera, L., Lopez, M., Patel, M., Louro, J., et al., 2012. The therapeutic profile of rolipram, PDE target and mechanism of action as a neuroprotectant following spinal cord injury. PLoS One 7, e43634.

Sebastiani, G., Morissette, C., Lagace, C., Boule, M., Ouellette, M.J., McLaughlin, R.W., Lacombe, D., et al., 2006. The cAMP-specific phosphodiesterase 4B mediates Abeta-induced microglial activation. Neurobiol. Aging 27, 691–701.

Koopmans, G.C., Deumens, R., Buss, A., Geoghegan, L., Myint, A.M., Honig, W.H., Kern, N., et al., 2009. Acute rolipram/thalidomide treatment improves tissue sparing and locomotion after experimental spinal cord injury. Exp. Neurol. 216, 490–498.

Whitaker, C.M., Beaumont, E., Wells, M.J., Magnuson, D.S., Hetman, M., Onifer, S.M., 2008. Rolipram attenuates acute oligodendrocyte death in the adult rat ventrolateral funiculus following contusive cervical spinal cord injury. Neurosci. Lett. 438, 200–204.

Iannotti, C.A., Clark, M., Horn, K.P., van Rooijen, N., Silver, J., Steinmetz, M.P., 2011. A combination immunomodulatory treatment promotes neuroprotection and locomotor recovery after contusion SCI. Exp. Neurol. 230, 3–15.

Costa, L.M., Pereira, J.E., Filipe, V.M., Magalhaes, L.G., Couto, P.A., Gonzalo-Orden, J.M., Raimondo, S., et al., 2013. Rolipram promotes functional recovery after contusive thoracic spinal cord injury in rats. Behav. Brain Res. 243, 66–73.

Beaumont, E., Whitaker, C.M., Burke, D.A., Hetman, M., Onifer, S.M., 2009. Effects of rolipram on adult rat oligodendrocytes and functional recovery after contusive cervical spinal cord injury. Neuroscience 163, 985–990.

Blake, J.A., Eppig, J.T., Kadin, J.A., Richardson, J.E., Smith, C.L., Bult, C.J., the Mouse Genome DataBase Group, 2017. Mouse Genome Database (MGD)-2017: community knowledge resource for the laboratory mouse. Nucleic Acids Res. 45 (D1), D723–D729.

Benton, R.L., Maddie, M.A., Minnillo, D.R., Hagg, T., Whittemore, S.R., 2008. Griffonia simplicifolia isolectin B4 identifies a specific subpopulation of angiogenic blood vessels following contusive spinal cord injury in the adult mouse. J. Comp. Neurol. 507, 1031–1052.

Mahoney, E.T., Benton, R.L., Maddie, M.A., Whittemore, S.R., Hagg, T., 2009. ADAM8 is selectively up-regulated in endothelial cells and is associated with angiogenesis after spinal cord injury in adult mice. J. Comp. Neurol. 512, 243–255.

Scheff, S.W., Rabchevsky, A.G., Fugaccia, I., Main, J.A., Lumpp Jr., J.E., 2003. Experimental modeling of spinal cord injury: characterization of a force-defined injury device. J. Neurotrauma 20, 179–193.

Basso, D.M., Fisher, L.C., Anderson, A.J., Jakeman, L.B., McTigue, D.M., Popovich, P.G., 2006. Basso Mouse Scale for locomotion detects differences in recovery after spinal cord injury in five common mouse strains. J. Neurotrauma 23, 635–659.

Beare, J.E., Morehouse, J.R., Devries, W.H., Enzmann, G.U., Burke, D.A., Magnuson, D.S., Whittemore, S.R., 2009. Gait analysis in normal and spinal contused mice using the TreadScan system. J. Neurotrauma 26, 2045–2056.

Beare, J.E., Morehouse, J.R., Magnuson, D.S., Whittemore, S.R., 2011. Automated gait analysis following spinal cord injury. In: Chen, J. (Ed.), Animal Models of Acute Neurological Injuries. Humana, Totowa, NJ.

Gobejishvili, L., Avila, D.V., Barker, D.F., Ghare, S., Henderson, D., Brock, G.N., Kirpich, I.A., et al., 2011. S-adenosylmethionine decreases lipopolysaccharide-induced phosphodiesterase 4B2 and attenuates tumor necrosis factor expression via cAMP/protein kinase A pathway. J. Pharmacol. Exp. Ther. 337, 433–443.

Magnuson, D.S., Lovett, R., Coffee, C., Gray, R., Han, Y., Zhang, Y.P., Burke, D.A., 2005. Functional consequences of lumbar spinal cord contusion injuries in the adult rat. J. Neurotrauma 22, 529–543.

Myers, S.A., Devries, W.H., Andres, K.R., Gruenthal, M.J., Benton, R.L., Hoying, J.B., Hagg, T., et al., 2011. CD47 knockout mice exhibit improved recovery from spinal cord injury. Neurobiol. Dis. 42, 21–34.

Whetstone, W.D., Hsu, J.Y., Eisenberg, M., Werb, Z., Noble-Haeusslein, L.J., 2003. Blood-spinal cord barrier after spinal cord injury: relation to revascularization and wound healing. J. Neurosci. Res. 74, 227–239.

Fassbender, J.M., Myers, S.A., Whittemore, S.R., 2011. Activating Notch signaling post-

SCI modulates angiogenesis in penumbral vascular beds but does not improve hindlimb locomotor recovery. Exp. Neurol. 227, 302–313.

Donnelly, D.J., Gensel, J.C., Ankeny, D.P., van Rooijen, N., Popovich, P.G., 2009. An efficient and reproducible method for quantifying macrophages in different experimental models of central nervous system pathology. J. Neurosci. Methods 181, 36–44.

Aagaard, K., Petrosino, J., Keitel, W., Watson, M., Katancik, J., Garcia, N., Patel, S., et al., 2013. The Human Microbiome Project strategy for comprehensive sampling of the human microbiome and why it matters. FASEB J. 27, 1012–1022.

Gevers, D., Knight, R., Petrosino, J.F., Huang, K., McGuire, A.L., Birren, B.W., Nelson, K.E., et al., 2012. The Human Microbiome Project: a community resource for the healthy human microbiome. PLoS Biol. 10, e1001377.

Caporaso, J.G., Lauber, C.L., Walters, W.A., Berg-Lyons, D., Huntley, J., Fierer, N., Owens, S.M., et al., 2012. Ultra-high-throughput microbial community analysis on the Illumina HiSeq and MiSeq platforms. ISME J. 6, 1621–1624.

Caporaso, J.G., Kuczynski, J., Stombaugh, J., Bittinger, K., Bushman, F.D., Costello, E.K., Fierer, N., et al., 2010. QIIME allows analysis of high-throughput community sequencing data. Nat. Methods 7, 335–336.

Lenth, R.V., 2006-2009. Java Applets for Power and Sample size [Computer software].

Duricki, D.A., Soleman, S., Moon, L.D., 2016. Analysis of longitudinal data from animals with missing values using SPSS. Nat. Protoc. 11, 1112–1129.

Atkins, C.M., Oliva Jr., A.A., Alonso OF, Pearse, D.D., Bramlett, H.M., Dietrich, W.D., 2007. Modulation of the cAMP signaling pathway after traumatic brain injury. Exp. Neurol. 208, 145–158.

Pearse, D.D., Pereira, F.C., Marcillo, A.E., Bates, M.L., Berrocal, Y.A., Filbin, M.T., Bunge, M.B., 2004. cAMP and Schwann cells promote axonal growth and functional recovery after spinal cord injury. Nat. Med. 10, 610–616.

Pilakka-Kanthikeel, S., Huang, S., Fenton, T., Borkowsky, W., Cunningham, C.K., Pahwa, S., 2012. Increased gut microbial translocation in HIV-infected children persists in virologic responders and virologic failures after antiretroviral therapy. Pediatr. Infect. Dis. J. 31, 583–591.

Avila, D.V., Myers, S.A., Zhang, J., Kharebava, G., McClain, C.J., Kim, H.Y., Whittemore, S.R., et al., 2017. Phosphodiesterase 4b expression plays a major role in alcohol-induced neuro-inflammation. Neuropharmacology 125, 376–385.

Lakatos, P.L., Kiss, L.S., Palatka, K., Altorjay, I., Antal-Szalmas, P., Palyu, E., Udvardy, M., et al., 2011. Serum lipopolysaccharide-binding protein and soluble CD14 are markers of disease activity in patients with Crohn's disease. Inflamm. Bowel Dis. 17, 767–777.

Krizsan-Agbas, D., Winter, M.K., Eggimann, L.S., Meriwether, J., Berman, N.E., Smith, P.G., McCarson, K.E., 2014. Gait analysis at multiple speeds reveals differential functional and structural outcomes in response to graded spinal cord injury. J. Neurotrauma 31, 846–856.

Gungor, B., Adiguzel, E., Gursel, I., Yilmaz, B., Gursel, M., 2016. Intestinal microbiota in patients with spinal cord injury. PLoS One 11, e0145878.

Carding, S., Verbeke, K., Vipond, D.T., Corfe, B.M., Owen, L.J., 2015. Dysbiosis of the gut microbiota in disease. Microb. Ecol. Health Dis. 26, 26191.

Pan, Y., Liu, B., Li, R., Zhang, Z., Lu, L., 2014. Bowel dysfunction in spinal cord injury: current perspectives. Cell Biochem. Biophys. 69, 385–388.

Schulz, C., Schutte, K., Malfertheiner, P., 2016. Helicobacter pylori and other gastric microbiota in gastroduodenal pathologies. Dig. Dis. 34, 210–216.

Bull-Otterson, L., Feng, W., Kirpich, I., Wang, Y., Qin, X., Liu, Y., Gobejishvili, L., et al., 2013. Metagenomic analyses of alcohol induced pathogenic alterations in the intestinal microbiome and the effect of Lactobacillus rhamnosus GG treatment. PLoS One 8, e53028.

Mutlu, E.A., Gillevet, P.M., Rangwala, H., Sikaroodi, M., Naqvi, A., Engen, P.A., Kwasny, M., et al., 2012. Colonic microbiome is altered in alcoholism. Am. J. Physiol. Gastrointest. Liver Physiol. 302, G966–G978.

Fernandez-Real, J.M., Lopez-Bermejo, A., Castro, A., Broch, M., Penarroja, G., Vendrell, J., Vazquez, G., et al., 2005. Opposite relationship between circulating soluble CD14 concentration and endothelial function in diabetic and nondiabetic subjects. Thromb. Haemost. 94, 615–619.

Gobejishvili, L., Barve, S., Joshi-Barve, S., McClain, C., 2008. Enhanced PDE4B expression augments LPS-inducible TNF expression in ethanol-primed monocytes: relevance to alcoholic liver disease. Am. J. Physiol. Gastrointest. Liver Physiol. 295, G718–G724.

Kleppisch, T., 2009. Phosphodiesterases in the central nervous system. Handb. Exp. Pharmacol. 71–92.

Wang, X., Baughman, K.W., Basso, D.M., Strittmatter, S.M., 2006. Delayed Nogo receptor therapy improves recovery from spinal cord contusion. Ann. Neurol. 60, 540–549.

Murphy DLA, C.S., Garrick, N.A., Sunderland, T., 1987. Monoamine oxidase inhibitors as antidepressants. In: Meltzer, H.Y. (Ed.), Psychopharmacology: The Third Generation of Progress. Raven Press, New York, pp. 545–552.

Southwood, C.M., Garbern, J., Jiang, W., Gow, A., 2002. The unfolded protein response modulates disease severity in Pelizaeus-Merzbacher disease. Neuron 36, 585–596.

Lin, F., Yu, C., Jiang, T., Li, K., Chan, P., 2007. Diffusion tensor tractography-based group mapping of the pyramidal tract in relapsing-remitting multiple sclerosis patients. AJNR Am. J. Neuroradiol. 28, 278–282.

Pennuto, M., Tinelli, E., Malaguti, M., Del Carro, U., D'Antonio, M., Ron, D., Quattrini, A., et al., 2008. Ablation of the UPR-mediator CHOP restores motor function and reduces demyelination in Charcot-Marie-Tooth 1B mice. Neuron 57, 393–405.

Ohri, S.S., Maddie, M.A., Zhao, Y., Qiu, M.S., Hetman, M., Whittemore, S.R., 2011. Attenuating the endoplasmic reticulum stress response improves functional recovery after spinal cord injury. Glia 59, 1489–1502.

Narazaki, M., Kishimoto, T., 2018. The two-faced cytokine IL-6 in host defense and diseases. Int. J. Mol. Sci. 19, 1–28.

Scheller, J., Chalaris, A., Schmidt-Arras, D., Rose-John, S., 2011. The pro- and anti-inflammatory properties of the cytokine interleukin-6. 1813. pp. 878–888.

Ohri, S.S., Hetman, M., Whittemore, S.R., 2013. Restoring endoplasmic reticulum homeostasis improves functional recovery after spinal cord injury. Neurobiol. Dis. 58, 29–37.

Komatsu, K., Lee, J.Y., Miyata, M., Hyang Lim, J., Jono, H., Koga, T., Xu, H., et al., 2013. Inhibition of PDE4B suppresses inflammation by increasing expression of the deubiquitinase CYLD. Nat. Commun. 4, 1684.

Gurney, M.E., D'Amato, E.C., Burgin, A.B., 2015. Phosphodiesterase-4 (PDE4) molecular pharmacology and Alzheimer's disease. Neurotherapeutics 12, 49–56.

Housley, M.D., Schafer, P., Zhang, K.Y., 2005. Keynote review: phosphodiesterase-4 as a therapeutic target. Drug Discov. Today 10, 1503–1519.

Bretzner, F., Plemel, J.R., Liu, J., Richter, M., Roskams, A.J., Tetzlaff, W., 2010. Combination of olfactory ensheathing cells with local versus systemic cAMP treatment after a cervical rubrospinal tract injury. J. Neurosci. Res. 88, 2833–2846.

Gonzalez-Garcia, C., Bravo, B., Ballester, A., Gomez-Perez, R., Eguiluz, C., Redondo, M., Martinez, A., et al., 2013. Comparative assessment of PDE 4 and 7 inhibitors as therapeutic agents in experimental autoimmune encephalomyelitis. Br. J. Pharmacol. 170, 602–613.

Singh, V., Roth, S., Llovera, G., Sadler, R., Garzetti, D., Stecher, B., Dichgans, M., Liesz, A., 2016. Microbiota dysbiosis controls the neuroinflammatory response after stroke. Neuro Dis. 36, 7428–7440.

Wang, Y., Kirpich, I., Liu, Y., Ma, Z., Barve, S., McClain, C.J., Feng, W., 2011. Lactobacillus rhamnosus GG treatment potentiates intestinal hypoxia-inducible factor, promotes intestinal integrity and ameliorates alcohol-induced liver injury. Am. J. Pathol. 179, 2866–2875.

Wen, L., Duffy, A., 2017. Factors Influencing the Gut Microbiota, Inflammation, and Type 2 Diabetes. J. Nutr. 147, 1468S–1475S.

Holleran, G., Lopetuso, L.R., Ianiro, G., Pecere, S., Pizzoferrato, M., Petito, V., Graziani, C., et al., 2017. Gut microbiota and inflammatory bowel disease: an update. Minerva Gastroenterol. Dietol. 63 (4), 373–384. https://doi.org/10.23736/S1121-421X.17.02386-8. (Dec, PMID: 28293937).

Ji, Q., Di, Y., He, X., Liu, Q., Liu, J., Li, W., Zhang, L., 2016. Intrathecal injection of phosphodiesterase 4B-specific siRNA attenuates neuropathic pain in rats with L5 spinal nerve ligation. Mol. Med. Rep. 13, 1914–1922.

McGirr, A., Lipina, T.V., Mun, H.S., Georgiou, J., Al-Amri, A.H., Ng, E., Zhai, D., et al., 2016. Specific inhibition of phosphodiesterase-4B results in anxiolysis and facilitates memory acquisition. Neuropsychopharmacology 41, 1080–1092.